Recombination and resistive losses at ZnO / a-Si:H / c-Si interfaces in heterojunction back contacts for Si solar cells

Florian Einsele, Philipp J. Rostan, Markus B. Schubert, and Uwe Rau

Citation: Journal of Applied Physics **102**, 094507 (2007);
View online: https://doi.org/10.1063/1.2803749
View Table of Contents: http://aip.scitation.org/toc/jap/102/9
Published by the American Institute of Physics

Recombination and resistive losses at ZnO/*a*-Si:H/*c*-Si interfaces in heterojunction back contacts for Si solar cells

Florian Einsele, Philipp J. Rostan,[a] and Markus B. Schubert
Institut für Physikalische Elektronik (IPE), Universität Stuttgart, Pfaffenwaldring 47, 70569 Stuttgart, Germany

Uwe Rau[b]
IEF5-Photovoltaik, Forschungszentrum Jülich, 52425 Juelich, Germany

(Received 24 July 2007; accepted 11 September 2007; published online 6 November 2007)

We investigate resistive losses at *p*-type crystalline Si/hydrogen passivated Si:H/ZnO:Al heterojunction back contacts for high efficiency silicon solar cells. A low tunneling resistance for the (*p*-type) Si:H/(*n*-type) ZnO part of the junction requires deposition of Si:H with a high hydrogen dilution rate $R_H > 40$ resulting in a highly doped microcrystalline (μc) Si:H layer. Such a μc-Si:H layer if deposited directly on a Si wafer yields a surface recombination velocity of $S \approx 180$ cm/s. Using the same layer as part of a (*p*-type) *c*-Si/Si:H/ZnO:Al back contact in a solar cell results in an open circuit voltage $V_{OC} = 640$ mV and a fill factor FF=80%. Insertion of an undoped amorphous (*i*) *a*-Si:H layer between the μc-Si:H and the wafer leads to a further decrease of *S* and, for the solar cells, to an increase of V_{OC}. However, if the thickness of this intrinsic layer exceeds a threshold value of 4–5 nm, resistive losses degrade the fill factor FF of the solar cells. Temperature dependent measurements of the contact resistance unveil activation energies in a range of 0.49–0.65 eV, which we attribute to the valence band offset between *a*-Si:H and *c*-Si. The balance of FF losses and V_{OC} gains determines the optimum (*i*) *a*-Si:H interlayer thickness for (*i*) *a*-Si:H/(*p*) μc-Si:H double layer or (*i*) *a*-Si:H/(*p*) *a*-Si:H/(*p*) μc-Si:H triple layer back contacts. © *2007 American Institute of Physics*. [DOI: 10.1063/1.2803749]

I. INTRODUCTION

Heterojunction solar cells from crystalline Si (*c*-Si) and amorphous hydrogenated Si (*a*-Si:H) are a promising alternative to conventional solar cells from *c*-Si with diffused emitters.[1] One advantage of the heterojunctions is the much lower process temperatures required for the deposition of the *a*-Si:H layers as compared to those needed for dopant indiffusion. In addition, the thin intrinsic (i) *a*-Si:H layer introduced between the doped *a*-Si:H layers of the front and the back contacts and the *c*-Si absorber leads to a very low interface recombination velocity at both interfaces.[1–6]

When using *a*-Si:H/*c*-Si heterojunctions for the contacts to *c*-Si solar cell absorbers, the band alignment between the two materials plays a crucial role. There is wide agreement in literature on the fact that the *a*-Si:H/*c*-Si band offset mainly shows up in the valence band. Using different characterization methods, Refs. 7–11 report valence band offsets $\Delta E_V = 0.44 - 0.71$ eV, whereas the conduction band offset ΔE_C is found to be $\Delta E_C < 0.15$ eV in all cases. Because of this asymmetry in the band offsets, it is obviously much easier to extract electrons from the *c*-Si absorber into an *a*-Si:H contact than it is to extract holes. Sanyo's successful heterojunction with intrinsic thin layer (HIT) solar cell[1] uses a *n*-type doped *c*-Si absorber, an emitter consisting of an intrinsic and a *p*-type doped *a*-Si layer, and a corresponding *i*/*n*-type structure as the back contact. All these layers are deposited using plasma enhanced chemical vapor deposition (PECVD). In this structure, extraction of electrons, i.e., the majority carriers, into the back contact poses no problem because of the small value of ΔE_C. In contrast, upon using *p*-type *c*-Si absorbers, the extraction of holes into the *p*-type *a*-Si:H back contact becomes a challenge due to the large band offset ΔE_V in the valence band. Despite of this drawback, Ref. 4 reports highly efficient solar cells produced using *p*-type *c*-Si absorbers and a three-layer sequence (*i*) *a*-Si:H/(*p*) *a*-Si:H/(*p*) μc-Si:H combined with ZnO as the back contact. Nevertheless, the optimization of the *a*-Si:H heterojunction back contact on *p*-type *c*-Si needs a better understanding and a closer experimental investigation, especially the simultaneous requirement for a low recombination velocity of electrons *and* for a low contact resistance for holes realized by the same contact.

This paper presents a detailed study on resistive losses that occur during hole transport across the (*p*) *c*-Si/(*i*) *a*-Si:H heterojunction contacts and during transport across the (p^+) μc-Si:H/(*n*) ZnO tunnel junction. We demonstrate that a low tunneling resistance for the latter interface is achieved if the silicon is deposited by PECVD with a hydrogen dilution above a certain threshold value. We argue that this threshold dilution coincides with the threshold for microcrystalline growth.[12–16] We show further that the conductance of the (*p*) *c*-Si/(*i*) *a*-Si:H heterojunction critically depends on the (*i*) *a*-Si:H layer thickness. Since a certain thickness d_i of the (*i*) *a*-Si:H layer is necessary for the minimization of the interface recombination velocity for elec-

[a]Present address: Centrotherm Photovoltaics Technology GmbH, 78467 Konstanz, Germany.
[b]Author to whom correspondence should be addressed. Electronic mail: u.rau@fz-juelich.de

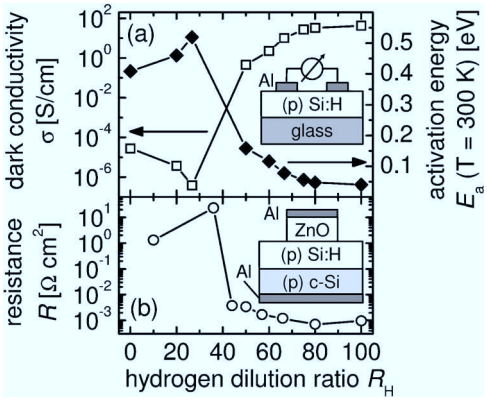

FIG. 1. (a) The room temperature dark conductivity σ and activation energy E_a of the conductivity samples exhibit a marked transition to higher σ and lower E_a values when the hydrogen dilution R_H during PECVD deposition of the Si:H layers exceeds a value of $R_H=40$. (b) Similarly, the resistance R of the tunnel junction test device drops by more than three orders of magnitude above $R_H=40$. The insets show the cross section of the respective sample structure.

trons, optimization of d_i for solar cells requires a compromise between the increase of series resistance and the decrease of recombination. This optimization problem is finally demonstrated by an investigation of the fill factors FF and the open circuit voltages V_{OC} of *c*-Si solar cells with various d_i within their back contact structure.

II. TUNNEL JUNCTION (*p*) Si:H/ZnO

This section concentrates on the relation between the bulk conductivity of the PECVD-deposited (*p*-type) Si:H layer, on the one side, and the tunneling resistance between the thin (*p*-type) Si:H and the *n*-type ZnO:Al, on the other side. For the characterization of the Si:H films, we measure their dark conductivity σ and the corresponding activation energy E_a. The junctions are analyzed by measuring the resistance R of a test structure. Both measurements are performed as a function of the hydrogen dilution ratio R_H during the deposition of the Si:H layers.

The conductivity samples consist of a 100 nm layer of boron doped Si:H deposited on Corning® borosilicate glass. For this deposition step, we use a gas mixture of 2% B_2H_6 in SiH_4 and vary the hydrogen dilution ratio $R_H=H_2/SiH_4$. The plasma frequency ν_p during PECVD deposition is $\nu_P=80$ MHz (VHF). The samples are finished by evaporation of Al contacts through shadow masks directly onto the Si:H surface, producing coplanar, 1 cm wide electrodes with a gap of 1 mm. The inset of Fig. 1(a) shows a cross section of the samples. For the measurement, we vary the sample temperature T and measure the current I at constant applied voltage V between two electrodes, using a Keithley 617 electrometer. From the known geometry of the sample and the measured values of I, we derive the temperature dependent dark conductivity $\sigma(T)=\sigma_0 \exp(-E_a/kT)$, with the preexponential factor σ_0, the activation energy E_a, and the thermal energy kT. Because of the temperature dependence of the activation energy, we use the method of Ref. 17 with a value of $\sigma_0=200$ S/cm to extract the value E_a ($T=300$ K) at room temperature.

Figure 1(a) shows the dark conductivity σ at room temperature $T=300$ K and the activation energy E_a ($T=300$ K) depending on the hydrogen dilution ratio R_H of the samples. We observe a significant step of more than four orders of magnitude in conductivity σ when the hydrogen dilution exceeds a threshold at $R_H\approx 40$. At the same time, the activation energy E_a decreases due to a higher doping and/or a higher fraction of activated boron atoms in the Si:H layer. This behavior and the increased conductivity suggest a transition from amorphous to microcrystalline growth of the Si:H layer under high hydrogen dilutions and VHF plasma frequencies.[13] For dilution ratios $R_H>40$, the conductivity σ increases further and reaches values up to $\sigma>20$ S/cm. This finding is consistent with earlier results on the crystallinity of PECVD Si:H films deposited under similar conditions, where the authors report an increased crystalline fraction for increased hydrogen dilutions during deposition.[13,14]

Next we investigate the resistance of samples consisting of a tunneling contact between hydrogen diluted Si:H and *n*-type ZnO. For this purpose, we use a test structure [see inset of Fig. 1(b)] consisting of 40 nm layer of boron doped Si:H directly deposited onto the surface of highly doped ($\rho\approx 10-20$ mΩ cm) *p*-type *c*-Si wafers. All deposition parameters are chosen identical to those used for the conductivity samples, and we again vary the hydrogen dilution ratio R_H during PECVD deposition. The test devices are finished by sputter deposition of a 40 nm ZnO:Al layer and by evaporation of Al contacts on both sides of the wafer. The Al contact on the back of the wafer is a full area contact, whereas the Al contact on top of the Si:H is evaporated through a shadow mask onto areas of 0.1 cm^2. Subsequently, we remove ZnO between the contact pads by a short etch in 1% HCl solution. An annealing step of 10 min at 220 °C completes the procedure. We measure the current-voltage curve of the samples using a Keithley 2400 source measurement unit and obtain the resistance R from the derivation of the curve.

Figure 1(b) shows the functional dependence of the zero-bias resistance R of the tunnel junction test device on the hydrogen dilution ratio R_H. For the resistance R we observe a significant step by more than three orders of magnitude when the hydrogen dilution exceeds the threshold value of $R_H\approx 40$. This matches well our results from dark conductivity measurements and supports the theory of microcrystalline growth associated with higher effective doping. For dilution ratios $R_H>40$ the resistance decreases down to $R<10^{-3}$ Ω cm^2. This value is by far low enough to avoid any significant resistive losses in heterojunction solar cells. In contrast, for dilution ratios $R_H<40$, the contact resistance is pronouncedly too high for usage in a solar cell.

III. HETEROJUNCTION *c*-Si/(*i*)*a*-Si:H

Insertion of an (*i*) *a*-Si:H interlayer between the highly doped μc-Si:H and the *c*-Si absorber is desirable to reduce interface recombination.[3,5,6] However, this layer also introduces additional resistive losses that finally require a tradeoff between low recombination and low contact resistance. In order to study the effect of interlayer thickness d_i on the contact resistance of the *c*-Si/(*i*) *a*-Si:H/μc-Si:H/ZnO het-

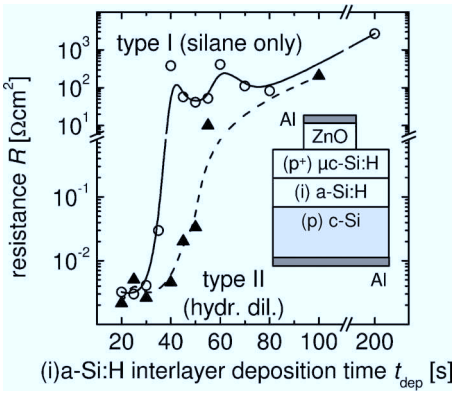

FIG. 2. The resistance R of the heterojunction back contact increases sharply if a critical deposition time t_{dep} of the passivating (i) a-Si:H interlayer is exceeded. The critical time depends on whether only silane (type I) or an additional hydrogen dilution (type II) is used. The lines are guides to the eye. The inset sketches the device geometry.

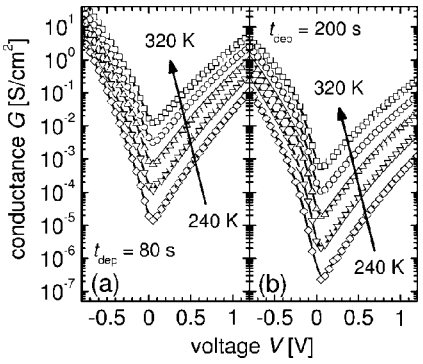

FIG. 3. Conductance G vs voltage V characteristics of heterojunction back contacts at different temperatures T=320, 300, 280, 260, and 240 K. The deposition times t_{dep} for the (i) a-Si:H interlayer (type I, without additional H_2) are t_{dep}=80 s (a) and t_{dep}=200 s (b). The polarity corresponds to the voltage applied to the Al contact on the c-Si wafer (cf. inset of Fig. 2).

erojunction, we fabricate samples with various deposition times t_{dep} of the (i) a-Si:H layer. The test structures as shown in the inset of Fig. 2 are essentially the same as those for analyzing the Si:H/ZnO tunnel resistance except for the (i) a-Si:H interlayer.

For the deposition of the (i) a-Si:H layers, we use either no H_2 added to the process gas (type I) or a hydrogen dilution ratio of R_H=2.5 (type II) and the standard rf plasma frequency of ν_P=13.56 MHz. The deposition rates measured from approximately 100 nm thick films grown on glass substrate are $r_I \approx 7.5$ nm/min for type I and $r_{II} \approx 5.5$ nm/min for type II films. In all these test structures, a 40 nm thick μc-Si:H layer grown with hydrogen dilution R_H=100 warrants a low tunneling resistance to the ZnO back contact.

Figure 2 shows the contact resistance R as a function of the deposition time t_{dep} for the two different films. For deposition times $t_{dep} \geqslant 30$ s, we obtain resistances $R < 10^{-2}\ \Omega\,\mathrm{cm}^2$ for both types of contacts, i.e., values that are well suited for a low-Ohmic back contact in a solar cell. At t_{dep}=35 s (type I) and 50 s (type II), the resistance R remains below $10^{-1}\ \Omega\,\mathrm{cm}^2$ before rather abruptly exceeding $10\ \Omega\,\mathrm{cm}^2$ and, thus, leaving the range of a reasonably low series resistance for a solar cell.

By using the growth rates extrapolated from the growth of thicker films on glass substrates, we deduce the critical thickness to be $d_i \approx 4-5$ nm for both types I and II of (i) a-Si:H deposition. We have to keep in mind, that the growth rate of a-Si:H on a c-Si substrate is likely to be larger than on a glass substrate.[18] In addition, the conditions for the growth of the first monolayers differ from those for bulk growth, resulting in a thickness-dependent deposition rate.[19,20] However, the good agreement of the critical thicknesses obtained for the different types of (i) a-Si:H substantiates the value of about $d_i \approx 4-5$ nm.

In order to gain insight into the nature of the resistive losses that arise from thicker (i) a-Si:H layers, we measure temperature dependent current/voltage (J/V) characteristics of the heterojunction back contact samples. These measurements are conducted in a nitrogen-cooled cryostat. For the analysis we differentiate the J/V characteristics to obtain the conductance $G=dJ/dV$ as a function of voltage V and temperature T.

Figures 3(a) and 3(b) display such $G(V)$ characteristics of two samples having an (i) a-Si:H layer deposited without hydrogen dilution (type I). The samples correspond to deposition times t_{dep}=80 s [Fig. 3(a)] and 200 s [Fig. 3(b)]. For both samples, we clearly see a diodelike asymmetry with the forward direction given by the negative polarity applied to the Al contact on the c-Si wafer. Thus, injection of holes from the μc-Si:H layer over the (i) a-Si:H interlayer into the c-Si wafer is easier than the extraction of holes from the wafer. This finding indicates that the barrier between the highly doped c-Si wafer and the (i) a-Si:H interlayer is higher than that between μc-Si:H and the (i) a-Si:H layer. Since the Fermi energies E_F in both highly doped Si materials (the c-Si wafer and the μc-Si:H layer) are close to the valence band energy E_V, we may identify the barrier at either side of the (i) a-Si:H layer with the respective valence band offsets ΔE_V. As can be seen from the comparison of Figs. 4(a) and 4(b), the larger band offset ΔE_V at the c-Si/(i) a-Si:H interface compared to ΔE_V at the μc-Si:H/(i) a-Si:H interface explains the asymmetry of the $G(V)$ characteristics in Fig. 3.

To separately investigate the μc-Si:H/(i) a-Si:H inter-

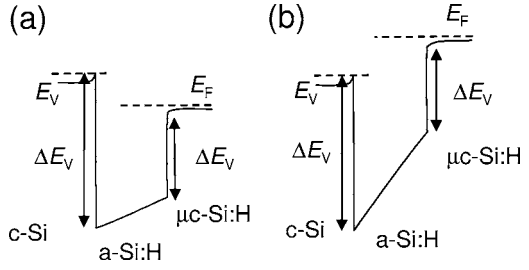

FIG. 4. Band diagram (valence band energy E_V only) of the c-Si/(i) a-Si:H/μc-Si:H heterojunctions from Figs. 2 and 3. The forward direction of the current flow (a) corresponds to a negative bias applied to the c-Si wafer. Here the Fermi energy E_F on the c-Si side is above that on the μc-Si:H side, such that holes travel from the right to the left. In reverse direction (b) the hole current from the c-Si side is hampered by the valence band offset ΔE_V between the c-Si wafer and the (i) a-Si:H interlayer. This band offset is higher than ΔE_V between the μc-Si:H and the (i) a-Si:H.

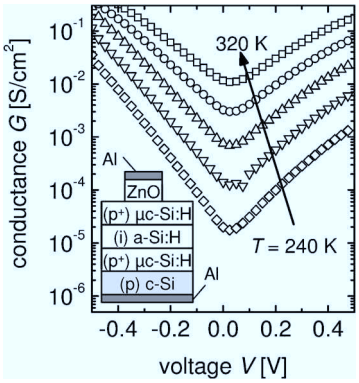

FIG. 5. Conductance G vs voltage V characteristics of a μc-Si:H/(*i*) *a*-Si:H/μc-Si:H structure as shown in the inset. The measurements are performed at temperatures T=320, 300, 280, 260, and 240 K. The deposition times t_{dep} for the (*i*) *a*-Si:H interlayer (type I, without additional H_2) is t_{dep}=150 s.

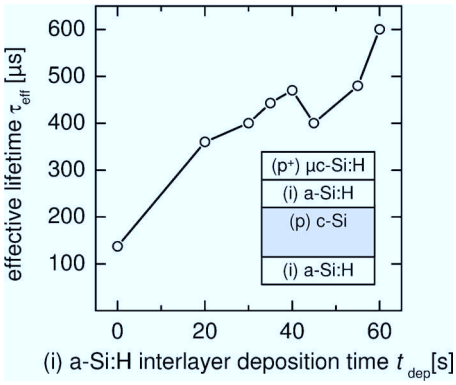

FIG. 7. The effective lifetime τ_{eff} increases with increasing deposition time t_{dep} for the (*i*) *a*-Si:H passivating interlayer between the crystalline wafer and the (p^+)μc-Si layer. The inset sketches a cross section of our samples with a 30 nm of passivating (*i*) *a*-Si:H layer on the back side. The straight line is a guide to the eye.

face, we fabricate structures that contain an additional 40 nm thick μc-Si:H layer between the *c*-Si substrate and the (*i*) *a*-Si:H interlayer. As sketched in the inset of Fig. 5, the (*i*) *a*-Si:H layer (deposition time t_{dep}=150 s) is sandwiched between two μc-Si:H layers. The corresponding G/V characteristics in Fig. 5 are more symmetric than the corresponding curves in Fig. 3. However, the conductance is markedly higher when injecting holes from the μc-Si:H layer adjacent to the ZnO (cf. inset in Fig. 5). Obviously, the deposition sequence has a non-negligible influence on the electronic properties of the respective interfaces.

To investigate the barrier heights for the heterocontact systems of Figs. 3(a), 3(b), 5(a), and 5(b), we analyze the thermal activation of the zero-bias conductance G_0 for these samples. Figure 6(a) depicts an Arrhenius plot of G_0 of *c*-Si/(*i*) *a*-Si:H/μc-Si:H samples (inset of Fig. 3) for *a*-Si:H interlayer deposition times t_{dep}=50, 80, and 200 s. From the fits to the data, we obtain the activation energies E_a=0.49, 0.57, and 0.65 eV, respectively. If we identify E_a with the valence band offset ΔE_V between the *c*-Si wafer and the (*i*) *a*-Si:H interlayer, this result corresponds reasonably well to the band offset data reported earlier.[8–11] In view of such a high band offset it appears impossible to achieve a low-Ohmic contact without the support of additional transport paths. In fact, back contacts with $t_{dep} \leqslant 35$ s and $R \leqslant 10^{-1}\ \Omega\,\mathrm{cm}^2$ at T=300 K (cf. Fig. 2) exhibit nonlinear or only partially linear Arrhenius plots [not shown in Fig. 3(a)], where no distinct value for E_a can be extracted. Here, several possible processes offer an explanation and are possibly superimposed: (i) quantum-mechanical tunneling through the few nanometer thin potential barrier; (ii) lateral inhomogeneities of the (*i*) *a*-Si:H layer due to initially insular growth of the amorphous intrinsic layer[13] resulting in laterally inhomogenous tunneling probabilities and/or uncovered domains; (iii) hydrogen etching of the (*i*) *a*-Si:H layer during deposition of the μc-Si:H, known in literature as preferential etching of the amorphous phase[21–23] that would have similar consequences.

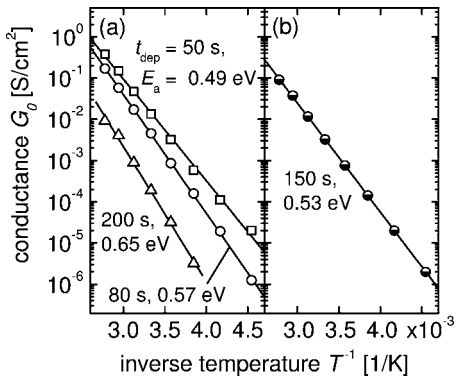

FIG. 6. (a) The Arrhenius plots of the zero-bias conductance G_0 of the heterojunction back contacts demonstrate an increase of the activation energies E_a with increasing deposition time t_{dep} of the (*i*) *a*-Si:H layer. (b) Arrhenius plot for G_0 of a μc-Si:H/(*i*) *a*-Si:H/μc-Si:H sandwich structure as sketched in the inset of Fig. 5 exhibiting an activation energy E_a =0.53 eV.

Figure 6(b) shows the Arrhenius plot of the zero-bias conductance G_0 versus T^{-1} obtained from the data in Fig. 5 exhibiting an activation energy E_a=0.53 eV. This value is smaller than E_a obtained from the asymmetric structures with comparable deposition times for the (*i*) *a*-Si:H layer in Fig. 6(a). Thus, we conclude that the valence band offset between (*i*) *a*-Si:H and *c*-Si is about 100 meV larger than the one between (*i*) *a*-Si:H and μc-Si:H. This difference explains the asymmetry of the G/V characteristics in Fig. 3. Using the transitivity rule, we additionally conclude that the valence band offset ΔE_V between μc-Si:H and *c*-Si is about 100 meV. A value of $\Delta E_V \approx 100$ meV also explains that the resistance measurements depicted in Fig. 2 exhibit no transport barrier between *c*-Si and μc-Si:H.

IV. LIFETIME MEASUREMENTS

This section studies the influence of the (*i*) *a*-Si:H deposition time t_{dep} on the surface recombination velocity of 250 μm thick, 100 mm diameter, *p*-type float-zone Si wafers with resistivity $\rho \approx 1\ \Omega$ cm. The inset of Fig. 7 sketches the cross section of these samples being passivated one side with 30 nm thick (*i*) *a*-Si:H and on the other one with (*i*) *a*-Si:H layers of various deposition times followed by the highly doped μc-Si:H layer (R_H=100, ν_P=80 MHz).

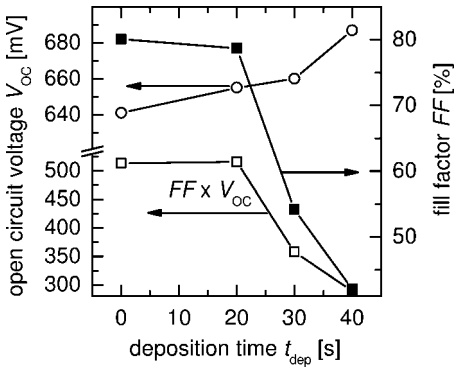

FIG. 8. Open circuit voltage V_{OC} and fill factor FF of solar cells with a (*i*) *a*-Si:H/(*p*) μc-Si:H double layer heterostructure back contact depending on the (*i*) *a*-Si:H deposition time t_{dep}. The product $V_{OC}\times$FF for the double layer back contact exhibits no maximum for a finite deposition time t_{dep}.

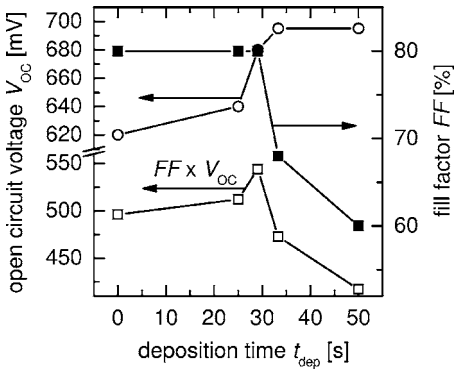

FIG. 9. Open circuit voltage V_{OC} and fill factor FF of solar cells with a (*i*) *a*-Si:H/(*p*) *a*-Si:H/(*p*) μc-Si:H triple layer heterostructure back contact depending on the (*i*) *a*-Si:H deposition time t_{dep}. The product $V_{OC}\times$FF for the triple layer system exhibits a clear maximum at a deposition time t_{dep} =30 s.

The effective minority carrier lifetime $\tau_{eff}=1\pm0.1$ ms is determined by the quasi-steady-state photoconductance method[24] for reference wafers covered with (*i*) *a*-Si:H layers of 30 nm thickness on each side. Assuming negligible bulk recombination, we derive a surface recombination velocity $S\approx13$ cm/s using the model of Sproul.[25] For the asymmetric structures depicted in the inset of Fig. 7, the effective lifetime increases from 100 μs [for no (*i*) *a*-Si:H interlayer] up to 600 μs (after a deposition time $t_{dep}=60$ s). Accepting $S\approx13$ cm/s for the side passivated with 30 nm (*i*) *a*-Si:H, we find values between $S=180$ cm/s and $S=30$ cm/s for the side passivated with the (*i*) *a*-Si:H/(*p*) μc-Si:H double layer. First of all, there seems to be a reasonable surface passivation quality for any thickness of the (*i*) *a*-Si:H layer and even when omitting it. This result is in contrast to the work of de Wolf and Beaucarne[26] who found that the passivation quality of 3 nm thin (*i*) *a*-Si:H layers is destroyed by deposition of an additional (*p*) *a*-Si:H layer grown without hydrogen dilution. The high hydrogen dilution $R_H=100$ together with the VHF plasma frequency $\nu_p=80$ MHz that we use for our doped μc-Si:H layers obviously makes this difference. From the present results we see that increasing the deposition time for the (*i*) *a*-Si:H interlayer decreases the surface recombination velocity. Whether or not the simultaneous increase of the contact resistance compensates the expected efficiency gain is investigated in the next section.

V. SOLAR CELLS

To study the influence of the (*i*) *a*-Si:H thickness on the performance of *a*-Si:H back contacts for solar cells, we use test devices fabricated from 250 μm thick *p*-type Si wafers (resistivity $\rho\approx1\ \Omega$ cm) with a diffused emitter and a random pyramid texture at the front surface. For the (*i*) *a*-Si:H layer we use no hydrogen dilution (type I in Fig. 2), and we again vary the thickness of this interlayer.

Figure 8 depicts the open circuit voltages V_{OC} and fill factors FF of the completed cells as well as the product FF $\times V_{OC}$. Firstly, we see from Fig. 8 that already without an (*i*) *a*-Si:H interlayer, we obtain a $V_{OC}=640$ mV. Insertion of the (*i*) *a*-Si layer between the μc-Si:H and the wafer leads to an increase of V_{OC} with increasing interlayer thickness (expressed as deposition time t_{dep} in Fig. 8). A maximum $V_{OC}=687$ mV is achieved after a deposition time $t_{dep}=40$ s. However, the intrinsic layer leads to a decrease of the fill factor FF with increasing thickness d_i. As can be seen from Fig. 8, the fill factor drops dramatically from 78.7% to below 60% between $t_{dep}=20$ s and $t_{dep}=30$ s. This loss clearly overcompensates the simultaneous gain of few millivolts in V_{OC}. We use the product FF$\times V_{OC}$ as a figure of merit because the variations of the short circuit current density J_{SC} due to slight differences in the optical properties of the different cells are too large to allow us the use of the output power $P=J_{SC}\times$FF$\times V_{OC}$ for the same purpose. As can be seen from Fig. 8, the product FF$\times V_{OC}$ does barely change from $t_{dep}=0$ to $t_{dep}=20$ s and drops steeply for larger values of t_{dep} because of the decline of the fill factor.

From Fig. 8, we conclude that there is no real benefit from the (*i*) *a*-Si:H interlayer when directly combined with the μc-Si:H contact layer. In contrast, our best back contacts use an additional (*p*) *a*-Si:H layer prepared at $R_H=80$ and $\nu_P=13.56$ MHz (Ref. 4) in between the intrinsic passivation layer and the μc-Si:H contact layer. Figure 9 depicts the dependence of V_{OC}, FF, and FF$\times V_{OC}$ on the intrinsic layer deposition time. Here, the increase of V_{OC} with increasing t_{dep} is more pronounced than in Fig. 4, whereas the decline of FF at $t_{dep}>20$ s is less dramatic as for the two layer system. For the (*i*) *a*-Si:H/(*p*) *a*-Si:H/(*p*) μc-Si:H three-layer system of Fig. 9, we actually find a maximum for FF$\times V_{OC}$ around $t_{dep}=30$ s that combines a high $V_{OC}=680$ mV with a high fill factor FF=78.7% corresponding to a confirmed efficiency $\eta=21\%$, as reported in Ref. 4.

VI. CONCLUSIONS

The present study on resistive losses at (*p*) *c*-Si/(*p*) Si:H/(*n*) ZnO heterojunction back contacts for high efficiency silicon solar cells has demonstrated that a low tunneling resistance for the (*p*) Si:H/(*n*) ZnO part of the junction requires deposition of Si:H with a high hydrogen dilution $R_H>40$ resulting in a highly doped μc-Si:H layer. Such a μc-Si:H layer if deposited directly on a Si wafer yields already a relatively low surface recombination velocity of $S\approx180$ cm/s. Thus, using the same layer as part of a (*p*) *c*-Si/(*p*) Si:H/(*n*) ZnO back contact in a solar cell results in

an open circuit voltage $V_{OC}=640$ mV and a fill factor FF $=80\%$. Insertion of an additional (i) a-Si:H layer between the μc-Si:H and the wafer leads to a further decrease of S and, for the solar cells, to an increase of V_{OC}. However, if the thickness d_i of this intrinsic layer exceeds a threshold of $d_i \approx 4-5$ nm, resistive losses cause a degradation of the fill factor FF of the solar cells. These FF losses overcompensate the V_{OC} gain such that there is no real benefit of the (i) a-Si:H interlayer for the overall solar cell performance when using an (i) a-Si:H/(p) μc-Si:H double layer. In contrast, the triple-layer system (i) a-Si:H/(p) a-Si:H/(p) μc-Si:H used for our earlier solar cells[4] exhibits a maximum performance at a nonzero (i) a-Si:H interlayer thickness. The reason for the critical dependence of the series resistance and the fill factor of the solar cells on the (i) a-Si:H layer lies in the relatively large valence band offsets ΔE_V at the c-Si/(i) a-Si:H interface ($\Delta E_V \approx 650$ meV) and at the μc-Si/(i) a-Si:H interface ($\Delta E_V \approx 530$ meV).

ACKNOWLEDGMENTS

The authors are grateful to J. H. Werner (IPE) and W. Beyer (FZ Jülich) for helpful discussions and critical remarks.

[1] M. Taguchi, K. Kawamoto, S. Tsuge, T. Baba, H. Sakata, M. Morizane, K. Uchihashi, N. Nakamura, S. Kiyama, and O. Oota, Prog. Photovoltaics **8**, 503 (2000).
[2] N. Jensen, U. Rau, R. M. Hausner, S. Uppal, L. Oberbeck, R. B. Bergmann, and J. H. Werner, J. Appl. Phys. **87**, 2639 (2000).
[3] N. Jensen, R. M. Hausner, R. B. Bergmann, J. H. Werner, and U. Rau, Prog. Photovoltaics **10**, 1 (2002).
[4] P. J. Rostan, U. Rau, V. X. Nguyen, T. Kirchartz, M. B. Schubert, and J. H. Werner, Sol. Energy Mater. Sol. Cells **90**, 1345 (2006).
[5] H. Plagwitz, M. Nerding, N. Ott, H. P. Strunk, and R. Brendel, Prog. Photovoltaics **12**, 47 (2004).
[6] M. Schaper, J. Schmidt, H. Plagwitz, and R. Brendel, Prog. Photovoltaics **13**, 381 (2005).
[7] H. Mimura and Y. Hatanaka, Appl. Phys. Lett. **50**, 326 (1987).
[8] J. M. Essick and J. D. Cohen, Appl. Phys. Lett. **55**, 1232 (1989).
[9] J. M. Essick, Z. Nobel, Y.-M. Li, and M. S. Bennett, Phys. Rev. B **54**, 4885 (1996).
[10] M. Schmidt, L. Korte, A. Laades, R. Stangl, Ch. Schubert, H. Angermann, E. Conrad, and K. v. Maydell, Thin Solid Films **515**, 7475 (2007).
[11] M. Sebastiani, L. Di Gaspare, G. Capellini, C. Bittencourt, and F. Evangelisti, Phys. Rev. Lett. **75**, 3352 (1995).
[12] R. W. Collins and B. Y. Yang, J. Vac. Sci. Technol. B **7**, 1155 (1989).
[13] H. Keppner, J. Meier, P. Torres, D. Fischer, and A. Shah, Appl. Phys. A: Mater. Sci. Process. **69**, 169 (1999).
[14] M. Tzolov, F. Finger, R. Carius, and P. Hapke, J. Appl. Phys. **81**, 7376 (1997).
[15] L. Houben, M. Luysberg, P. Hapke, R. Carius, F. Finger, and H. Wagner, Philos. Mag. A **77**, 1447 (1998).
[16] E. Amanatides, D. Mataras, and D. E. Rapakoulias, J. Appl. Phys. **90**, 5799 (2001).
[17] J. Stuke, J. Non-Cryst. Solids **97–98**, 1 (1987).
[18] W. Westlake and M. Heintze, J. Appl. Phys. **77**, 879 (1995).
[19] H. Fujiwara and M. Kondo, Appl. Phys. Lett. **86**, 032112 (2005).
[20] H. Fujiwara and M. Kondo, Appl. Phys. Lett. **90**, 013503 (2007).
[21] F. Finger, P. Hapke, M. Luysberg, R. Carius, H. Wagner, and M. Scheib, Appl. Phys. Lett. **65**, 2588 (1994).
[22] M. Heintze, W. Westlake, and P. V. Santos, J. Non-Cryst. Solids **166**, 985 (1993).
[23] C. Godet and B. Drévillon, J. Vac. Sci. Technol. A **6**, 2482 (1988).
[24] R. A. Sinton and A. Cuevas, Appl. Phys. Lett. **69**, 2510 (1996).
[25] A. B. Sproul, J. Appl. Phys. **76**, 2851 (1994).
[26] S. De Wolf and G. Beaucarne, Appl. Phys. Lett. **88**, 022104 (2006).